Journal of Peptide Science
J. Pept. Sci. 2008; **14**: 118–126
Published online 16 November 2007 in Wiley InterScience (www.interscience.wiley.com). DOI: 10.1002/psc.955

JOURNAL OF PEPTIDE SCIENCE

Sequence shuffle controls morphological consequences in a self-assembling tetrapeptide‡

K. B. JOSHI and SANDEEP VERMA*
Department of Chemistry, Indian Institute of Technology Kanpur, Kanpur-208 016 (UP), India

Received 31 May 2007; Revised 18 August 2007; Accepted 13 September 2007

Abstract: Peptide and protein self-assembly is a well-studied phenomenon in chemistry and biology, where nanoscopic building blocks exhibit rapid self-association to reveal supramolecular aggregates of defined structural features. These superstructures are stabilized by hydrophobic interactions, hydrogen bonding and a host of other noncovalent interactions. Thus, amino acid side chains in the primary structure hold importance in dictating secondary structures and preference for particular conformational signatures in peptide aggregates. This report describes contrasting nanoscale morphologies in antamanide-derived synthetic tetrapeptide mutants, which are composed by shuffling only two amino acids: phenylalanine and proline. Remarkable differences in ultrastructures in primary sequence-shuffled tetrapeptides suggest dissimilar aggregational pathways due to context-dependent location of proline and phenylalanine residues with respect to one another. Copyright © 2007 European Peptide Society and John Wiley & Sons, Ltd.

Supplementary electronic material for this paper is available in Wiley InterScience at http://www.interscience.wiley.com/jpages/1075-2617/suppmat/

Keywords: peptide; self-assembly; tetrapeptide; $\pi-\pi$ interactions; antamanide

INTRODUCTION

Peptide-based self-assembled structures respond to a variety of factors such as pH, ionic strength, concentration, and hydrophobicity and hydrophilicity of amino acid side-chains [1–5]. Such external stimuli alter nucleation mechanisms in self-assembled structures and affect the propagation step, thereby triggering observable variations in the morphological features. With an aim to generate structures of required morphologies, the study and control of parameters governing structural transformations has become an area of contemporary interest [6–8].

Aromatic $\pi-\pi$ interactions are crucial for three-dimensional structures and functions of proteins [9–11]. For example, these interactions were implicated for stability and directionality to amyloid self-assembly and influence fibril morphology [12–14]. In this vein, properties of a peptide fragment KLVFFA, as a crucial recognition motif in Aβ aggregation, is well documented [15,16]. It has been proposed that FF aromatic dipeptide may serve as a minimal motif mimicking the aggregation properties of the Aβ protein [17–21].

Antamanide, a naturally occurring cyclic decapeptide, inhibits the uptake of bile salts by hepatocytes and this activity is attributed to the Pro-Phe-Phe tripeptide sequence (Figure 1) [22–24]. Karle and coworkers have extensively reported on the channel-like solid state structure of antamanide in the presence or absence of metal ions [25–27]. We decided to study the aggregation of truncated antamanide sequences containing phenylalanine residue(s) to determine if the shuffling of aromatic residues, with respect to proline, will have an impact on ensuing ultrastructural morphologies. Our interest in this work emanates from our recent studies dealing with the self-assembly of short peptide sequences, including the ones containing aromatic amino acids [28–36].

MATERIAL AND METHODS

General

Dichloromethane; N, N-dimethylformamide; methanol; triethylamine; and 1, 2-dimethoxy ethane were distilled following standard procedures. Trifluoroacetic acid; N, N′-dicyclohexylcarbodiimide; N-hydroxybenzotriazole; di-*tert*-butyl-pyrocarbonate; sodium hydroxide; diethyl ether; and L-amino acids were purchased from Spectrochem, Mumbai, India, and used without further purification. ^{1}H and ^{13}C NMR spectra were recorded on JEOL-JNM LAMBDA 400 model operating at 400 and 100 MHz, respectively. Mass spectra were recorded at RSIC, Lucknow, India on JEOL SX 102/DA-6000 mass spectrometer data system using Argon/Xenon (6 kV, 10 mA) as the FAB gas. Elemental analyses (C, H, N) were performed on Perkin-Elmer 240-C automatic elemental analyzer.

* Correspondence to: Sandeep Verma, Department of Chemistry, Indian Institute of Technology Kanpur, Kanpur-208 016 (UP), India;
e-mail: sverma@iitk.ac.in
‡ This article is part of the Special Issue of the Journal of Peptide Science entitled "Peptides in Nanotechnology".

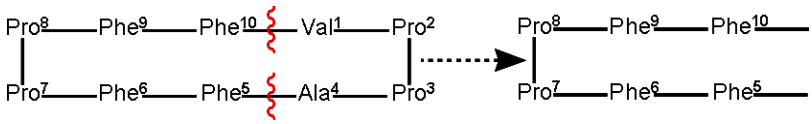

Figure 1 Antamanide, a naturally occurring cyclic decapeptide (curved lines indicate truncation sites). This figure is available in colour online at www.interscience.wiley.com/journal/jpepsci.

Peptide Synthesis

All tetrapeptides were synthesized by simple solution phase fragment condensation methodologies using *t*-Boc chemistry and in the presence of HOBt. Purity of final deprotected products was checked by analytical FPLC [Amersham Pharmacia FPLC system (Akta Basic), using a μRPC C2/C18 ST 4.6/100 column (Pharmacia Biotech) with an applied gradient of 0.1% trifluoroacetic acid in water (eluent A) to 0.1% trifluoroacetic acid in acetonitrile (eluent B) (20–80% in 20 min). Concentration of a peptide for a typical analytical run was ~1 mg/ml] and satisfactory analytical spectroscopic results were also obtained for all the samples. Details of peptide syntheses are described in the supporting information.

Atomic Force Microscopy (AFM)

Fresh peptide samples were imaged with an atomic force microscope (Molecular Imaging, USA) operating under Acoustic AC (AAC) mode, with the aid of cantilever (NSC 12(c) from MikroMasch). The force constant was 0.6 N/m, while the resonant frequency was 150 kHz. The images were taken in air at room temperature, with a scan speed of 1.5–2.2 lines/s. The data acquisition was done using PicoScan 5 software, while the data analysis was done using visual SPM. Fresh solutions of 'tetrapeptides' (3 mM) in 50% methanol/water were prepared and micrographs were recorded. The tetrapeptides (3 mM) were incubated at 37 °C for 0–30 days in methanol/water and micrographs were recorded for selected incubation periods. Aqueous solution of 10 µl aliquot of these tetrapeptides was transferred onto freshly cleaved mica surface and uniformly spread using a spin-coater operating at 200–500 rpm (PRS-4000). The sample-coated mica was dried for 30 min at room temperature, followed by atomic force microscopy (AFM) imaging.

Scanning Electron Microscopy (SEM)

A 20 µl aliquot of the fresh peptide solution was dried at room temperature on a copper stub and coated with gold. Scanning electron microscopy (SEM) images were made using a FEI QUANTA 200 microscope equipped with a tungsten filament gun operating at WD 10.6 mm and 20 kV. Concentration of the peptide sample was 3 m M.

Transmission Electron Microscopy (TEM)

A 10 µl aliquot of the peptide solution after 10 and 30 days of incubation was placed on a 400 mesh copper grid. After 1 min, excess fluid was removed and the grid was stained with 2% uranyl acetate in water. The excess staining solution was removed from the grid after 2 min. Samples were viewed using a JEOL 1200EX electron microscope operating at 80 kV.

Fourier Transform Infrared Spectroscopy

Infrared spectra of peptide samples were recorded using a Bruker Vertex 70 Fourier transform infrared spectroscopy (FTIR) spectrometer with a resolution 4 cm^{-1}, scan speed 2.5 kHz, and 128 scans co-addition, in the KBr pellet form. The obtained spectra were smoothened by using the Savintky-Goolay algorithm to eliminate the noise and by operating second derivative transformations on the spectra. Peptide solutions were incubated at 37 °C for 30 days and then lyophilized. The deconvolution of the FTIR spectra was achieved using OPUS (Bruker) spectroscopic software.

RESULTS AND DISCUSSION

The morphological consequences in self-assembled structures of six truncated tetrapeptides, starting from the Phe5 residue of antamanide, were studied. The peptide sequences synthesized were: Phe5-Phe-Pro-Pro (**FFPP**), Phe6-Pro-Pro-Phe (**FPPF**), and Pro7-Pro-Phe-Phe (**PPFF**), and three scrambled tetrapeptide sequences: Pro-Phe-Phe-Pro (**PFFP**), Pro-Phe-Pro-Phe (**PFPF**), and Phe-Pro-Phe-Pro (**FPFP**) for control experiments (Figure 2). Interestingly, **PPFF**, **FFPP**, and **PFFP**, containing an FF dipeptide motif, displayed remarkably different ultrastructural morphologies upon aging in solution, while the other three peptides (**FPPF**, **PFPF**, **FPFP**) failed to display resolvable structures.

AFM with 10-day aged solutions of **PPFF, FFPP**, and **PFFP** in 50% aqueous methanol, revealed the emergence of three distinct morphologies (Figures 3(a–c)). **FFPP** afforded formation of circularly wound structures; aging of **PPFF** resulted in the formation of long fibers, while vesicular morphologies were observed for the **PFFP** tetrapeptide. The thickness of circular fibers from 10-day aged **FFPP** sample was determined to be 1 µm, while the fiber height (Z-scale) was 280 Å (Figure 3(a)). The thickness of straight tubular fibers from **PPFF** was 64 nm, with a height (Z-scale) of 34 Å and for **PFFP** vesicular structures, the thickness was ~1.2 µm, with height (Z-scale) of 560 Å (Figure 3(b–c)).

On prolonged incubation of 30 days, **FFPP** showed twisted fibrillar ring-like structures; aging of **PPFF** resulted in thicker fibers; while **PFFP** displayed a more dense vesicular morphology, signifying a direct effect of time dependence (Figure 3(d–f)). It is worth noting that a longer duration of incubation had no effect on the gross morphology of self-assembled tetrapeptides. The magnified 2D and 3D AFM micrographs of the three peptides at either 10 or 30 days of incubation present

DOI: 10.1002/psc

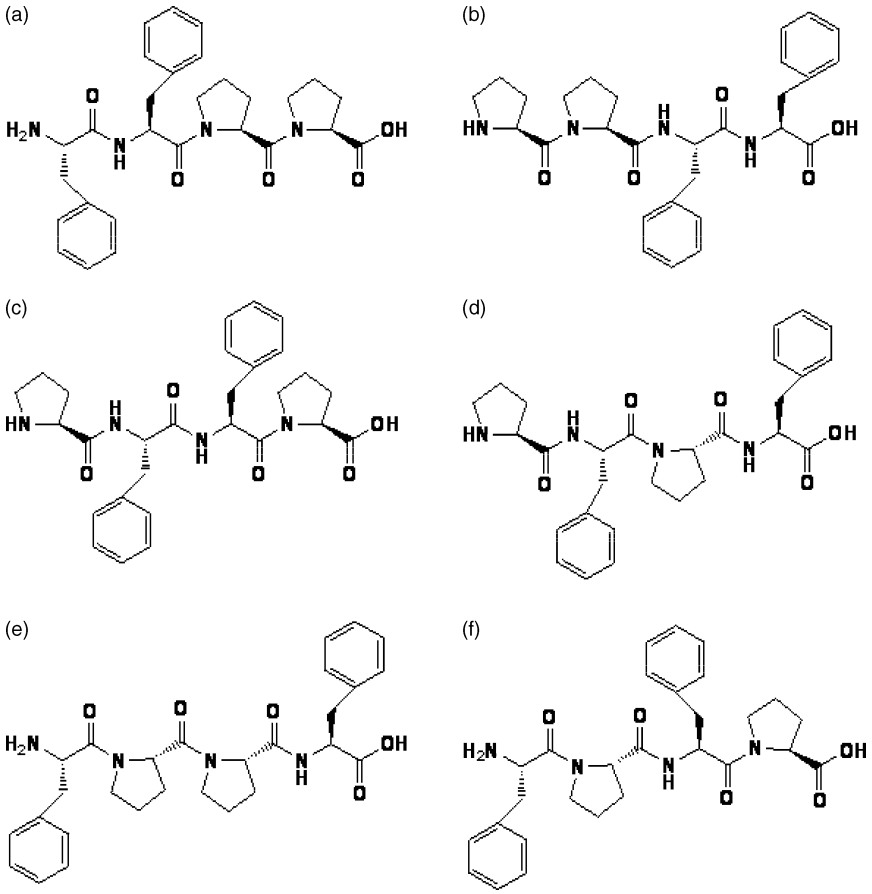

Figure 2 Molecular structures of (a) FFPP, (b) PPFF, (c) PFFP, (d) PFPF, (e) FPPF, and (f) FPFP.

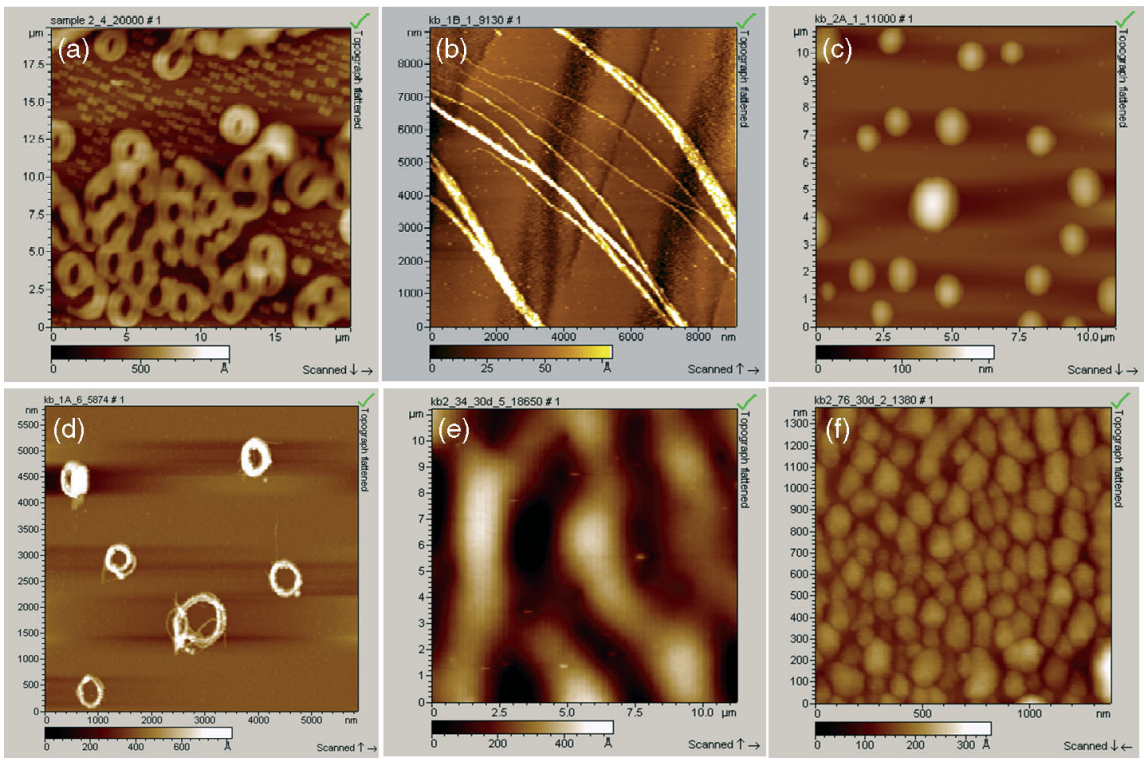

Figure 3 AFM micrograph of aged peptide samples in 50% aqueous methanol: (a, d) **FFPP**; (b, e) **PPFF**; and (c, f) **PFFP** (10- and 30-day aged samples for respective peptides at 37 °C).

DOI: 10.1002/psc

more resolvable features of the overall morphology (Figure 4). SEM and transmission electron microscopy (TEM) of aged samples further confirmed overall morphology of the ultrastructures observed in the AFM studies (Figure 5(a–f)).

Curiously, **FPPF**, **FPFP**, and **PFPF** did not form any resolvable structures. We observed that Pro-Pro dipeptide or Pro residues at either terminus was tolerable enough to support stable self-assembled structures, while Pro-Pro dipeptide flanked by phenylalanine on

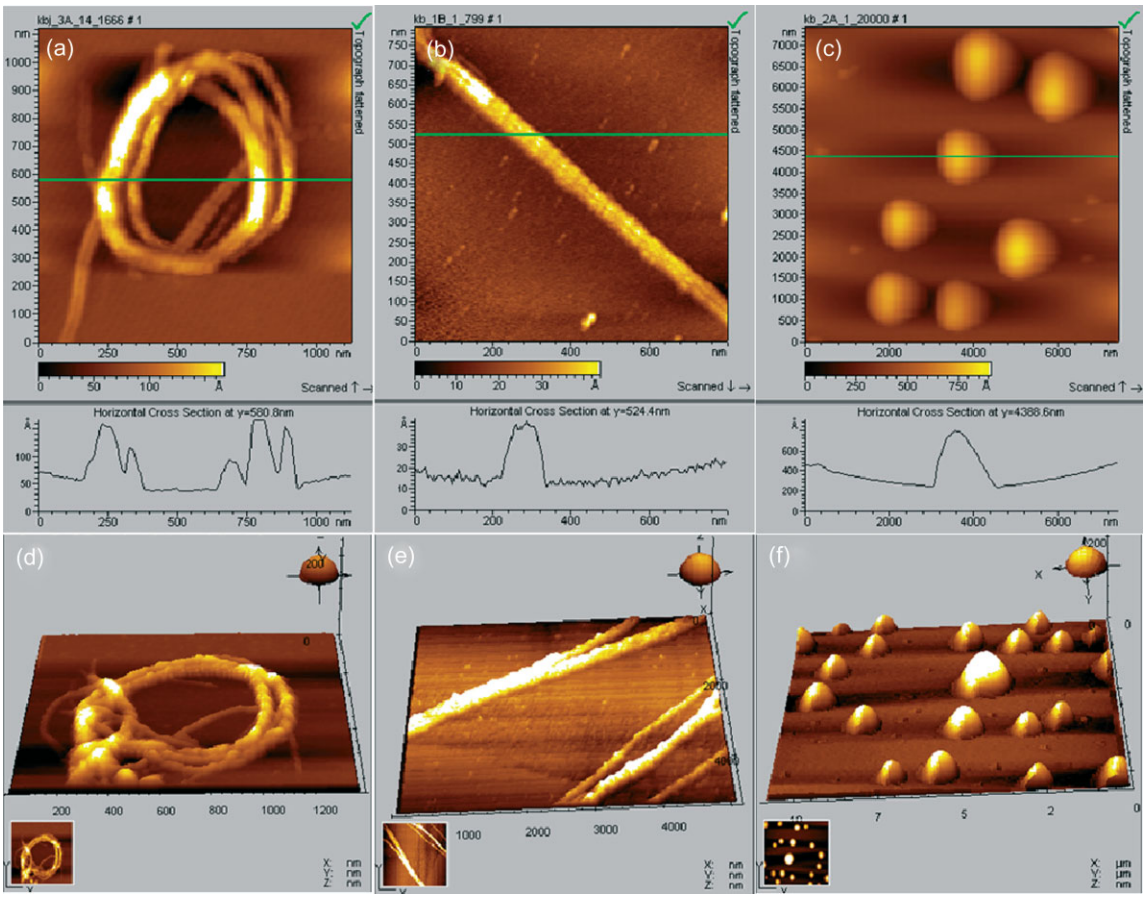

Figure 4 Magnified 2D and 3D AFM micrograph of aged tetrapeptides: (a, d) **FFPP** (30 days); (b, e) **PPFF** (10 days); and (c, f) **PFFP** (10 days).

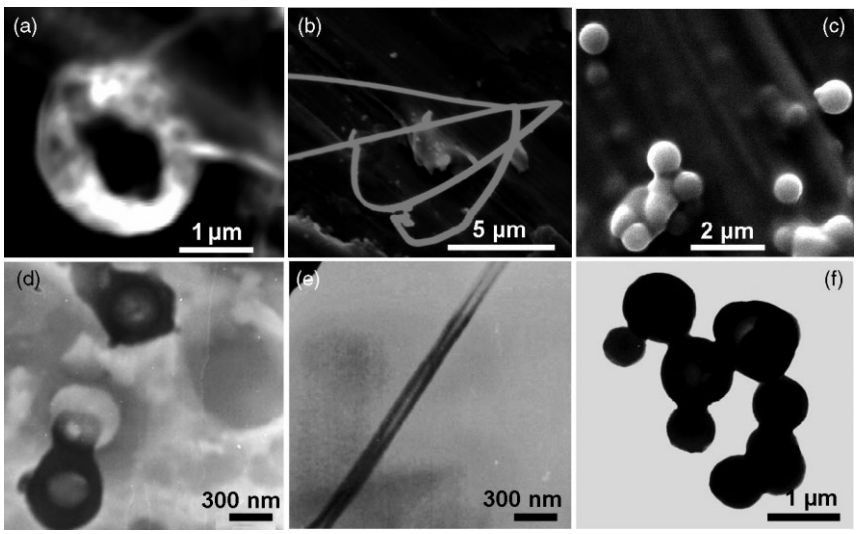

Figure 5 SEM micrographs (a–c) of 30-day aged tetrapeptides: (a) **FFPP**; (b) **PPFF**; (c) **PFFP**. TEM micrographs (d–f) of 10-day aged samples: (d) **FFPP**; (e) **PPFF**; (f) **PFFP**, respectively.

DOI: 10.1002/psc

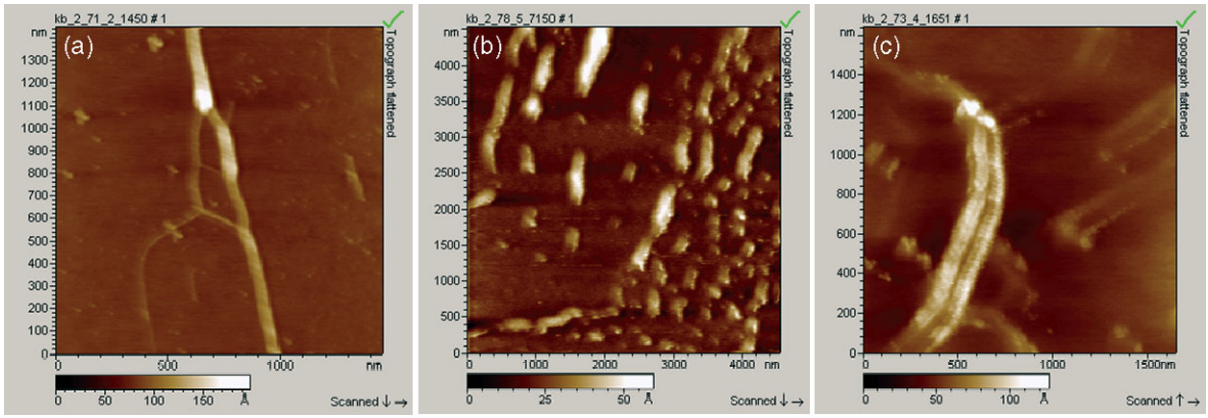

Figure 6 AFM micrographs of self-assembled aggregates of (a) **FPFP**, (b) **FPPF**, and (c) **PFPF** (10-day incubation at 37 °C).

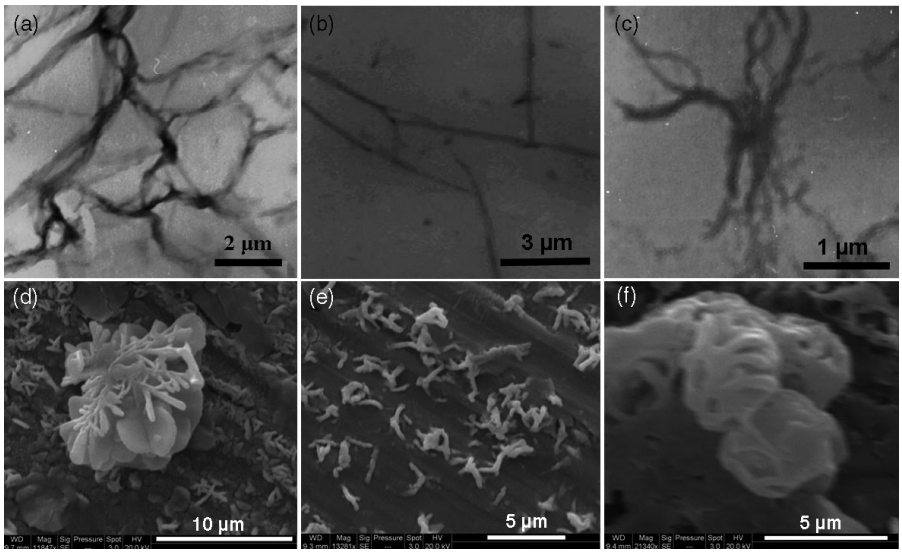

Figure 7 TEM and SEM micrographs of unresolved morphologies: (a, d) **FPFP**, (b, e) **FPPF**, and (c, f) **PFPF** (10-day incubation, 37 °C).

either side or when present in an alternating fashion in the tetrapeptide sequence, was not tolerated by the self-assembly process (Figures 6 and 7). Incidentally, structure-breaking and local conformational effects of proline residues have been described in literature [37–39]. However, Balaram and coworkers have presented an elegant elucidation of the role of diproline segments as folding nuclei in model peptides [40]. A number of conformations were detected in model studies and it was concluded that flanking residues and local environment effects may govern conformer distributions for the diproline segment.

Thus, it is reasonable to assume that overall morphology of the six tetrapeptides analyzed in this study is dictated by the aromatic interactions engendered in the diphenylalanine motif [6b], assisted by a subtle conformational control exerted by the diproline motif. The latter effect is especially significant for **PPFF** and **FFPP** peptides which revealed formation of stable self-assembled structures. A more detailed investigation of the possible interactions by NMR studies is required for a deeper structural understanding and to establish the precise role of the two amino acids in self-organization.

The self-assembly of N-Boc and ester protected tetrapeptides was also studied as control experiments. However, the protected derivatives failed to reveal resolvable nanostructures thus suggesting a crucial role of free *N*- and *C*-terminus peptides for the emergence of stable ultrastructural morphologies (Figure S2). Thus, it appears that the zwitterionic nature of peptides may be an important electrostatic consideration to arrive at defined morphologies in the cases described here. It is worth mentioning that the role of electrostatic interactions in diphenylalanine dipeptide self-assembly has been investigated by Gazit and Reches, where they concluded that aromatic interactions are prone to modulation by chemical modifications which change the net charged state of the dipeptide [41].

DOI: 10.1002/psc

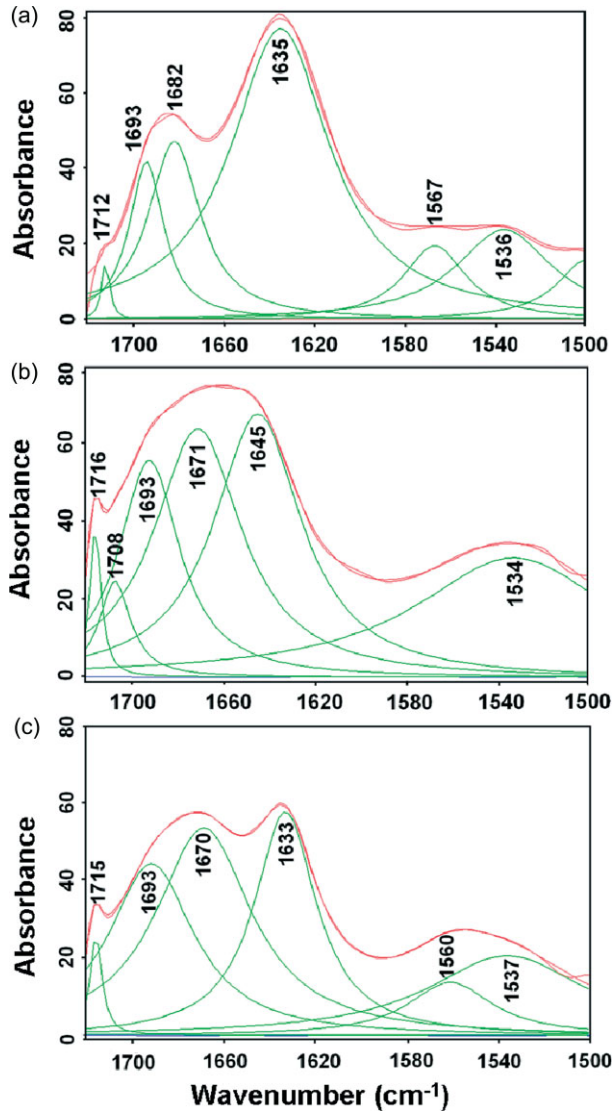

Figure 8 FTIR analyses of secondary structure of the studied tetrapeptides were analyzed from the second derivative of the infrared absorption spectra curve-fitting in the amide **I** and **II** region of (a) **FFPP**, (b) **PPFF**, and (c) **PFFP** tetrapeptides.

We resorted to FTIR spectroscopy to access information concerning the occurrence of various secondary structures in self-assembled peptide nanostructures described here [42–46]. Deconvolution and band-fitting of FTIR spectrum in the amide I and II regions of the three tetrapeptides displaying resolvable structures, **FFPP**, **PPFF**, and **PFFP** are shown in Figure 8. The amide I region of **FFPP** contains three components at 1693, 1682, and 1636 cm^{-1}, respectively. The absorption bands at 1636 and 1693 cm^{-1} are usually assigned to antiparallel β-sheets, while the band at 1682 cm^{-1} is indicative of random structures or β-turns. The deconvoluted amide II region of **FFPP** shows two components at 1567 and 1536 cm^{-1}, respectively, where the former band implicates a β-sheet conformation.

The amide I region for **PPFF** contains three component peaks at 1693, 1671, and 1645 cm^{-1}, respectively, which are assigned to antiparallel β-sheet conformation. Similarly, **PFFP** amide I bands at 1693 and 1670 cm^{-1} arise due to antiparallel β-sheets, and the one at 1633 cm^{-1} could be attributed to β-sheets or cross-β structures. From the overall deconvoluted FTIR data of these tetrapeptides, we can comment that β-sheets and related structures predominate resulting in the formation of discernable and resolvable aggregated nanostructures. Moreover, bands at 1712 (FFPP), 1716 and 1708 (PPFF), and 1715 cm^{-1} (PFFP), respectively, are attributed to free carboxylic acid group that have been previously implicated in peptide nanostructure formation and stabilization [47–50].

Fluorinated solvents exert considerable effect on stabilizing peptide and protein structures [51–53]. **FFPP**, **PPFF**, and **PFFP** were incubated in 50% aqueous trifluoroethanol and interestingly, the structures observed in aqueous methanol were retained in this solvent system suggesting that the persistent structures formed by these three sequences remain unaffected by change in the solvent composition (Figure 9).

Finally, we decided to construct a structural model to understand the possible reasons behind the emergence of three distinct morphological structures by amino acid shuffling in simple tetrapeptides. Model building for **FFPP** and **PPFF** fragments was directly achieved from antamanide crystal coordinates [25–27], while **PFFP** was separately modeled, following geometry optimization using the MM+ force field. Similar to the antamanide crystal structure, **PPFF** exhibited interaction between the aromatic and pyrrolidine rings (Figure 10), while **PFFP** and **FFPP** displayed a clear preference for aromatic stacking interactions (data not shown).

In the proposed model, **PPFF** molecules were stacked in columnar fashion in order to gain stability via aromatic–aromatic and pyrrolidine–aromatic interactions. Such an arrangement may be envisaged as a platform responsible for the growth of fibrous structures (Figure 10). Superimposition of a **PPFF** fiber observed in the AFM upon this columnar hierarchical model revealed that ~18 tetrapeptide molecules could fit in 163 Å long and 135 Å wide fibers.

A recent study by Koksch and coworkers nicely demonstrated a peptide construct achieving three different secondary structures, viz. random coil, β-sheet ribbons, and α-helical fibers, in response to pH and concentration variations [54]. It was suggested that such models may be used to study the influence of external factors on the peptide primary structure. Our results suggest that primary structure shuffle affects morphological consequences in the self-assembled structures. In the present case, structural variations are dictated by the relative position of Phe-Phe dipeptide *vis-à-vis* diproline motif through an intriguing interplay

DOI: 10.1002/psc

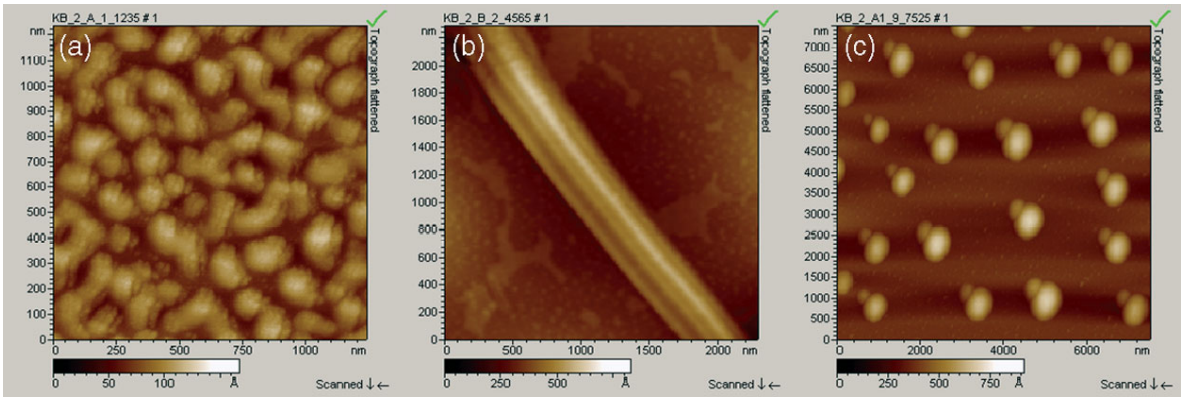

Figure 9 AFM micrographs of 10-day aged solutions of (a) **FFPP**, (b) **PPFF**, and (c) **PFFP** in 50% aqueous trifluoroethanol.

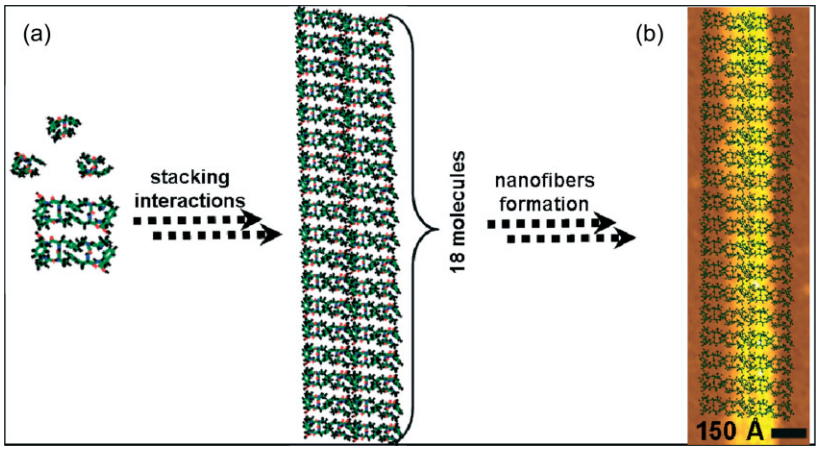

Figure 10 The proposed model for fiber formation by $\pi-\pi$ and pyrrolidine–aromatic interactions. (a) Structure of the truncated sequence PPFF is taken from the antamanide crystal structure, followed by geometry optimization using MM+ force field with the help of Hyperchem. (b) Superimposed AFM micrograph of PPFF.

of aromatic and pyrrolidine–aromatic interactions. We intend to elaborate these parameters for morphological transformations in other examples and by performing detailed solution phase studies. However, the present observations merit attention and we believe that such studies may lead to newer design paradigms for the generation of desired morphologies that can be predicted *a priori*.

CONCLUSIONS

This study illustrates a fascinating role of aromatic–aromatic and pyrrolidine–aromatic interactions in dictating aggregative ordering in a series of primary sequence-shuffled tetrapeptides. Microscopic evidences described here provide support for the aggregative propensity, while spectroscopic data reveals that the tetrapeptides quickly reach toward conformation(s) favoring antiparallel β-sheets or related structures, which are aided by aromatic–aromatic and pyrrolidine–aromatic interactions, leading to the emergence of a variety of peptide nanostructures. This study opens up new possibilities in understanding the role of primary sequence shuffling in peptide aggregation and as a design modality toward constructing interesting nanoscale motifs for advanced applications.

Supplementary Material

Supplementary electronic material for this paper is available in Wiley InterScience at: http://www.interscience.wiley.com/jpages/1075-2617/suppmat/

Acknowledgements

KBJ thanks IIT-Kanpur for a predoctoral research fellowship. This work is supported by a *Swarnajayanti Fellowship* in Chemical Sciences to SV from the Department of Science and Technology, India.

REFERENCES

1. Mart RJ, Osborne RD, Stevens MM, Ulijn RV. Peptide-based stimuli-responsive biomaterials. *Soft Matter* 2006; **2**: 822–835.

2. Rajagopal K, Ozbas B, Pochan DJ, Schneider JP. Probing the importance of lateral hydrophobic association in self-assembling peptide hydrogelators. *Eur. Biophys. J.* 2006; **35**: 162–169.
3. Dexter AF, Malcolm AS, Middelberg APJ. Reversible active switching of the mechanical properties of a peptide film at a fluid-fluid interface. *Nat. Mater* 2006; **5**: 502–506.
4. Paramonov SE, Jun HendashW, Hartgerink JD. Self-assembly of peptide-amphiphile nanofibers: The roles of hydrogen bonding and amphiphilic packing. *J. Am. Chem. Soc.* 2006; **128**: 7291–7298.
5. Zimenkov Y, Dublin SN, Ni R, Tu RS, Breedveld V, Apkarian RP, Conticello VP. Rational design of a reversible pH-responsive switch for peptide self-assembly. *J. Am. Chem. Soc.* 2006; **128**: 6770–6771, and references cited therein.
6. Zhao X, Zhang S. Molecular designer self-assembling peptides. *Chem. Soc. Rev.* 2006; **35**: 1105–1110.
7. Reches M, Gazit E. Molecular self-assembly of peptide nanostructures: mechanism of association and potential uses. *Curr. Nanosci.* 2006; **2**: 105–111.
8. Ryadnov MG, Woolfson DN. Engineering the morphology of a self-assembling protein fibre. *Nat. Mater* 2003; **2**: 329–332.
9. Waters ML. Aromatic interactions in peptides: Impact on structure and function. *Biopolymers* 2004; **76**: 435–445.
10. Claessens CG, Stoddart JF. $\pi-\pi$ Interactions in self-assembly. *J. Phys. Org. Chem.* 1997; **10**: 254–272.
11. Burley SK. Aromatic-aromatic interaction: a mechanism of protein structure stabilization. *Science* 1985; **229**: 23–28.
12. Marek P, Abedini A, Song B, Kanungo M, Johnson ME, Gupta R, Zaman W, Wong SS, Raleigh DP. Aromatic interactions are not required for amyloid fibril formation by islet amyloid polypeptide but do influence the rate of fibril formation and fibril morphology. *Biochemistry* 2007; **46**: 3255–3261.
13. Tartaglia GG, Cavalli A, Pellarin R, Caflisch A. The role of aromaticity, exposed surface, and dipole moment in determining protein aggregation rates. *Prot. Sci.* 2004; **13**: 1939–1941.
14. Gazit E. A possible role for π-stacking in the self-assembly of amyloid fibrils. *FASEB J.* 2002; **16**: 77–83.
15. Lowe TL, Strzelec A, Kiessling LL, Murphy RM. Structure-function relationships for inhibitors of beta-amyloid toxicity containing the recognition sequence KLVFF. *Biochemistry* 2001; **40**: 7882–7829.
16. Tjernberg LO, Callaway DJE, Tjernberg A, Hahne S, Lilliehook C, Terenius L, Thyberg J, Nordstedt C. A molecular model of Alzheimer amyloid β-peptide fibril formation. *J. Biol. Chem.* 1999; **274**: 12619–12625.
17. Gazit E. Mechanisms of amyloid fibril self-assembly and inhibition. Model short peptides as a key research tool. *FEBS Lett.* 2005; **272**: 5971–5978.
18. Reches M, Gazit E. Casting metal nanowires within discrete self-assembled peptide nanotubes. *Science* 2003; **300**: 625–627.
19. Azriel R, Gazit E. Analysis of the minimal amyloid-forming fragment of the islet amyloid polypeptide. An experimental support for the key role of the phenylalanine residue in amyloid formation. *J. Biol. Chem.* 2001; **276**: 34156–34161.
20. Görbitz CH. The structure of nanotubes formed by diphenylalanine, the core recognition motif of Alzheimer's β-amyloid polypeptide. *Chem. Commun.* 2006; **22**: 2332–2334.
21. Yan X, He Q, Wang K, Duan L, Cui Y, Li J. Transition of cationic dipeptide nanotubes into vesicles and oligonucleotide delivery. *Angew. Chem. Int. Ed. Engl.* 2007; **46**: 2431–2434.
22. Zanotti G, Rossi F, Saviano M, Tancredi T, Saviano G, Maione A, Filizola M, Blasio BD, Pedone C. A potent cyclolinopeptide A analog: Solid state and solution conformation of cyclo[Pro-Phe-Phe-Ala-Glu(OtBu)]$_2$. *J. Am. Chem. Soc.* 1995; **117**: 8651–8658.
23. Muenter K, Mayer D, Faulstich H. Characterization of a transporting system in rat hepatocytes. Studies with competitive and noncompetitive inhibitors of phalloidin transport. *Biochim. Biophys. Acta* 1986; **860**: 91–98.
24. Kessler H, Klein M, Muller A, Wagner K, Bats JW, Ziegler K, Frimmer M. Conformational prerequisites for the in vitro inhibition of cholate absorption in hepatocytes by cyclic antamanide and somatostatin analogs. *Angew. Chem. Int. Ed. Engl.* 1986; **25**: 997–999.
25. Karle IL, Wieland T, Schermer D, Ottenheym HCJ. Conformation of uncomplexed natural antamanide crystallized from acetonitrile/water. *Proc. Natl. Acad. Sci. U.S.A.* 1979; **76**: 1532–1536.
26. Karle I, Karle J, Wieland T, Burgermeister W, Witkop B. Conformation of uncomplexed [Phe4,Val6] antamanide crystallized from non-polar solvents. *Proc. Natl. Acad. Sci. U.S.A.* 1976; **73**: 1782–1785.
27. Karle IL, Karle J, Wieland T, Burgermeister W, Faulstich H, Witkop B. Conformations of the lithium-antamanide complex and sodium-[Phe4, Val6] antamanide complex in the crystalline state. *Proc. Natl. Acad. Sci. U.S.A.* 1973; **70**: 1836–1840.
28. Ghosh S, Reches M, Gazit E, Verma S. Bioinspired design of nanocages by self-assembling triskelion peptide elements. *Angew. Chem. Int. Ed. Engl.* 2007; **46**: 2002–2004.
29. Ghosh S, Singh SK, Verma S. Self-assembly and potassium ion triggered disruption of peptide-based soft structures. *Chem. Commun.* 2007; 2296–2298.
30. Joshi KB, Verma S. Monovalent cation-promoted ordering of a glycine-rich cyclic peptide. *Tetrahedron* 2007; **63**: 5602–5607.
31. Ghosh S, Verma S. Phased fiber growth in a peptide conjugate: Aggregation and disaggregation studies. *J. Phys. Chem. B* 2007; **111**: 3750–3757.
32. Prasad KK, Verma S. Ordering in a glycine-rich peptide conjugate: microscopic, fluorescence, and metalation studies. *Biopolymers* 2006; **83**: 289–296.
33. Joshi KB, Verma S. Ordered self-assembly of a glycine-rich linear and cyclic hexapeptide: contrasting ultrastructural morphologies of fiber growth. *Supramol. Chem.* 2006; **18**: 405–414.
34. Prasad KK, Purohit CS, Jain A, Sankararamakrishnan R, Verma S. Enforcing solution phase nanoscopic aggregation in a palindromic tripeptide. *Chem. Commun.* 2005; 2564–2566.
35. Madhavaiah C, Prasad KK, Verma S. Enforcing aggregation in a dipeptide conjugate. *Tetrahedron Lett.* 2005; **46**: 3745–3749.
36. Madhavaiah C, Verma S. Self-aggregation of reverse bis peptide conjugate derived from the unstructured region of the prion protein. *Chem. Commun.* 2004; 638–639.
37. Kim W, Hardcastle KI, Conticello VP. Fluorproline flip-flop: Regiochemical reversal of a stereoelectronic effect on peptide and protein structures. *Angew. Chem. Int. Ed. Engl.* 2006; **45**: 8141–8145.
38. Kim W, McMillan RA, Snyder JP, Conticello VP. A stereoelectronic effect on turn formation due to proline substitution in elastin-mimeti polypeptides. *J. Am. Chem. Soc.* 2005; **127**: 18121–18132.
39. Reiersen H, Rees AR. The hunchback and its neighbours: proline as an environmental modulator. *Trends Biochem. Sci.* 2001; **26**: 679–684.
40. Rai R, Aravinda S, Kanagarajadurai K, Raghothama S, Shamala N, Balaram P. Diproline templates as folding nuclei in designed peptides. Conformational analysis of synthetic peptide helices containing amino terminal Pro-Pro segments. *J. Am. Chem. Soc.* 2006; **128**: 7916–7928, references cited therein.
41. Reches M, Gazit E. Self-assembly of peptide nanotubes and amyloid-like structures by charged-termini-capped diphenylalanine peptide analogues. *Isr. J. Chem.* 2005; **45**: 363–371.
42. Reches M, Gazit E. Designed aromatic homo-dipeptides: formation of ordered nanostructures and potential nanotechnological applications. *Phys. Biol.* 2006; **3**: S10–S19.
43. Tamburro AM, Pepe A, Bochicchio B, Quaglino D, Ronchetti IP. Supramolecular amyloid-like assembly of the polypeptide sequence coded by exon30 of human tropoelastin. *J. Biol. Chem.* 2005; **280**: 2682–2690.
44. Valery C, Paternostre M, Robert B, Gulik-Krzywicki T, Narayanan T, Dedieu J-C, Keller G, Torres M-L, Cherif-Cheikh R, Calvo P, Artzner F. Biomimetic organization: Octapeptide self-assembly into nanotubes of viral capsid-like dimension. *Proc. Natl. Acad. Sci. U.S.A.* 2003; **100**: 10258–10262.

45. Aggeli A, Nyrkova IA, Bell M, Harding R, Carrick L, McLeish TCB, Semenov AN, Boden N. Hierarchical self-assembly of chiral rod-like molecules as a model for peptide β-sheet tapes, ribbons, fibrils, and fibers. *Proc. Natl. Acad. Sci. U.S.A.* 2001; **98**: 11857–11862.
46. Aggeli A, Bell M, Carrick LM, Fishwick CWG, Harding R, Mawer PJ, Radford SE, Strong AE, Boden N. pH as a trigger of peptide β-sheet self-assembly and reversible switching between nematic and isotropic phases. *J. Am. Chem. Soc.* 2003; **125**: 9619–9628.
47. Arrondo JL, Muga A, Castresana J, Goni FM. Quantitative studies of the structure of proteins in solution by Fourier-transform infrared spectroscopy. *Prog. Biophys. Mol. Biol.* 1993; **59**: 23–56.
48. Natalello A, Ami D, Brocca S, Lotti M, Doglia SM. Secondary structure, conformational stability and glycosylation of a recombinant Candida rugosa lipase studied by Fourier-transform infrared spectroscopy. *Biochem. J.* 2005; **385**: 511–517.
49. Saba RI, Ruysschaerr JM, Herchuelz A, Goormaghtigh E. Fourier transform infrared spectroscopy study of the secondary and tertiary structure of the reconstituted Na^+/Ca^{2+} exchanger 70-kDa polypeptide. *J. Biol. Chem.* 1999; **274**: 15510–15518.
50. Kogiso M, Hanada T, Yase K, Shimizu T. Intralayer hydrogen-bond-directed self-assembly of nano-fibers from dicarboxylic valylvaline bolaamphiphiles. *Chem. Commun.* 1998; **17**: 1791–1792.
51. Povey JF, smales CM, Hassard SJ, Howard MJ. Comparison of the effects of 2,2,2-trifluoroethanol on peptide and protein structure and function. *J. Struct. Biol.* 2007; **157**: 329–338.
52. Buck M. Trifluoroethanol and colleagues: Cosolvents come of age. Recent studies with peptides and proteins. *Q. Rev. Biophys.* 1998; **31**: 297–355.
53. Rajan R, Balaram P. A model for the interaction of trifluoroethanol with peptides and proteins. *Int. J. Pept. Protein Res.* 1996; **48**: 328–336.
54. Pagel K, Wagner SC, von Berlepsch H, Böttcher C, Koksch B. Random coils, beta-sheet ribbons, and alpha-helical fibers: one peptide adopting three different secondary structures at will. *J. Am. Chem. Soc.* 2006; **128**: 2196–2197.

DOI: 10.1002/psc